Available online at www.sciencedirect.com
ScienceDirect
Trans. Nonferrous Met. Soc. China 25(2015) 4216−4225
Transactions of Nonferrous Metals Society of China
www.tnmsc.cn

# Photocatalytic degradation of textile dyeing wastewater through microwave synthesized Zr−AC, Ni−AC and Zn−AC

P. SURESH[1], J. JUDITH VIJAYA[1], L. JOHN KENNEDY[2]

1. Catalysis and Nanomaterials Research Laboratory, Department of Chemistry, Loyola College, Chennai 600034, India;
2. Materials Division, School of Advanced Sciences, Vellore Institute of Technology University, Chennai Campus, Chennai 600048, India

Received 25 January 2015; accepted 4 July 2015

**Abstract:** The novel zirconium oxide, nickel oxide and zinc oxide nanoparticles supported activated carbons (Zr−AC, Ni−AC, Zn−AC) were successfully fabricated through microwave irradiation method. The synthesized nanoparticles were characterized using XRD, HR-SEM, XPS and BET. The optical properties of Zr−AC, Ni−AC and Zn−AC composites were investigated using UV–Vis diffuse reflectance spectroscopy. The photocatalytic efficiency was verified in the degradation of textile dyeing wastewater (TDW) in UV light irradiation. The chemical oxygen demand (COD) of TDW was observed at regular intervals to calculate the removal rate of COD. Zn−AC composites showed impressive photocatalytic enrichment, which can be ascribed to the enhanced absorbance in the UV light region, the effective adsorptive capacity to dye molecules, the assisted charge transfer and the inhibited recombination of electron−hole pairs. The maximum TDW degradation (82% COD removal) was achieved with Zn−AC. A possible synergy mechanism on the surface of Zn−AC was also designed. Zn−AC could be reused five times without exceptional loss of its activity.
**Key words:** nanostructure; semiconductor; textile dyeing wastewater; optical property; catalytic degradation

## 1 Introduction

Textile industries are facing an enormous issue of disposing textile effluents of high chemical oxygen demand (COD) content. Despite the extensive employment of traditional techniques like hydrolysis, chemical processes, membrane filtration, biological treatment and foam flotation, but still causes serious water contamination [1]. Hence, the need for new strategies and new technologies to mineralize textile−dyeing wastewater is the need of the hour. Nowdays, more than ever, heterogeneous photocatalysis has been envisaged as one of the environment friendly and effective strategies for wastewater treatment.

Sizable band gap semiconductor materials are being considered as photocatalyst for the degradation of textile dyes. $TiO_2$ is remarkably studied for such effects due to its high durability, inexpensiveness, high oxidizing capability and safe character [2]. ZnO is a profitable photocatalyst due to its broadband gap (3.2 eV) [3] and it is easily prepared with varied morphologies. Since it is secure and cost-effective, it has been used for the photocatalytic degradation of different dyes [4]. However, $TiO_2$ and ZnO were ineffective in large-scale treatment of dyes, due to inhibiting factors, like difficulty in recovery from the reaction mixture [5]. In order to avoid the drawback, $TiO_2$ and ZnO were mounted onto various supports, like activated carbon (AC) [6]. Activated carbon is an extremely employed adsorbent for textile wastewater treatment. Activated carbons are known for their large surface area, ordered porous structure and attractive forces towards dye molecules [7].

SURESH et al [8−10] have investigated the synergy mechanism in $ZrO_2$−AC, ZnO−AC and NiO−AC systems. In these studies, zero order kinetic fit was used for the photocatalytic degradation studies. However, in the present endeavor, $ZrO_2$, NiO and ZnO supported activated carbons (Zr−AC, Ni−AC and Zn−AC) composite catalysts were prepared by microwave irradiation. The composites were used for the photocatalytic degradation of textile-dyeing wastewater (TDW). The photocatalytic efficiency of the samples was compared using the pseudo first order kinetic fit, based

**Corresponding author:** J. JUDITH VIJAYA; Tel: +91-44-28178200, Fax: +91-44-28175566; E-mail: jjvijayaloyola@yahoo.co.in; jjvijaya78@gmail.com
DOI: 10.1016/S1003-6326(15)64072-9

on the removal rate of COD. The synergy mechanism behind the photocatalytic degradation was discussed in the light of TDW degradation studies. In view of industrial application, consideration will be given to durability, retrieval and reuse of the catalyst systems.

## 2 Experimental

### 2.1 Preparation of AC, Zr−AC, Ni−AC and Zn−AC

An activated carbon (AC) prepared by two-stage, two-step activation process was employed as support material [11]. The $ZrO_2$, NiO, and ZnO loaded activated carbons were prepared by microwave irradiation method. A fixed amount of AC was added to a metal nitrate solution and the suspension was stirred for 5 h. The mixture obtained was heated in a microwave (2.45 GHz, 750 W) for 10 min. After that, the solid was washed with distilled water to remove loosely bonded metal oxides and it was maintained in hot air oven at 100 °C for 1 h and was labeled as Zr−AC, Ni−AC and Zn−AC, respectively.

### 2.2 Characterization of AC, Zr−AC, Ni−AC and Zn−AC

The crystallinities of AC, Zr−AC, Ni−AC, and Zn−AC were analyzed by using a Philips X'pert X-ray diffractometer for $2\theta$ values ranging from 10° to 80° using Cu $K_\alpha$ radiation at $\lambda$=1.540 Å. Morphological analysis and energy dispersive X-ray analysis were done using a Jeol JSM6360 high resolution scanning electron microscope. X-ray photoelectron spectroscopy (XPS) test was performed (Make: Kratos analytical (UK), Model: Axis ultra) with a monochromatic Mg $K_\alpha$ X-ray source. The XPS curves of C 1s, O 1s and Zr 3d, Ni 2P, Zn 2P were deconvoluted into convenient number of peaks by using Gaussian fitting. The band gap energy of the samples was estimated from the data obtained from Cary100 UV−visible spectrophotometer. The specific surface area and porosity were evaluated from the surface area and porosity analyzer (ASAP 2020 V3.00H, Micromeritics Instrument Corp., Norcross, GA).

### 2.3 Photocatalytic reactor setup and degradation procedure

The entire photocatalytic degradations were executed at similar reaction parameters (initial concentration of TDW =1150 mg/L COD, wave length of UV light $\lambda$=365 nm). The textile dyeing wastewater (TDW) from local dyeing industry was taken in a multi lamp (low-pressure mercury lamps 8/8 W, $\lambda$=365 nm) photocatalytic reactor. An open borosilicate glass tube of 100 mL capacity was employed as a reaction vessel. The reaction mixture prior to photocatalytic degradation was kept in the dark overnight to attain adsorption–desorption equilibrium between TDW and photocatalyst. It was then placed in the photoreactor, an UV radiation of $\lambda$=365 nm was irradiated onto it. At routine spell of 20 min, equivalent aliquot was extracted from the reactor tube and centrifuged, and the COD was determined to observe the degradation of TDW. The standard dichromate method was employed to estimate the COD of TDW before and after the photocatalytic treatment. The removal rate ($\eta$) of COD was obtained from

$$\eta=(\text{initial COD} - \text{final COD/initial COD})\times 100\% \quad (1)$$

The Indian Pollution Control Board has prescribed COD limit of 250 mg/L as the discharge condition for TDW to be released into river bodies, hence the photocatalytic degradation of TDW was carried out using prepared catalyst to degrade TDW up to 250 mg/L COD.

## 3 Results and discussion

### 3.1 X-ray diffraction analysis

The XRD patterns of the AC, Zr−AC, Ni−AC and Zn−AC are shown in Fig. 1.

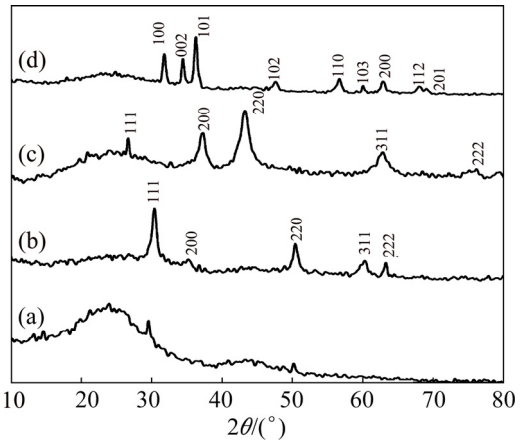


**Fig. 1** XRD patterns of AC (a), Zr−AC (b), Ni−AC (c) and Zn−AC (d)

In Fig. 1(a), a broad peak at a $2\theta$ value of 22°, and a small peak at 44° account for the presence of mineral $SiO_2$ and (010) planes of graphite structure, respectively [12]. Figure 1(b) shows the diffraction peaks of $ZrO_2$ at $2\theta$ values of 30.30°, 34.87°, 50.47°, 59.87° and 63.21° and exhibits the corresponding planes [111], [200], [220], [311] and [222], respectively (JCPDS No.02−0733) having tetragonal phase [13]. The planes conform to d-spacing standards of 2.93, 2.58, 1.80, 1.54 and 1.47 Å, appropriately. Figure 1(c) displays that the existence of peaks at $2\theta$ values of 44.51°, 51.85° and 76.36° is accounts for the presence of Ni and they correspond to (111), (200) and (220) planes, respectively (JCPDS 4−850, face-centered cubic phase). While, the peaks at

$2\theta$ values of 37.24°, 43.27°, 62.85°, 75.43° and 79.48° which can be indexed as (111), (200), (220), (311) and (222) crystal planes of NiO respectively (JCPDS file No. 4-835) have cubic phase. These planes of NiO are then linked with d-spacing standards of 2.40, 2.08, 1.47 and 1.24 Å fittingly. Figure 1(d) reveals that the existence of peaks at $2\theta$ angles of 31.58°, 34.41°, 36.21°, 47.56°, 56.58°, 63.03°, 66.39°, 68.19° and 69.21° is considered for the presence of ZnO and they agree to (100), (002), (101), (102), (110), (103) (200), (112) and (201) planes, respectively (JCPDS card No. 89—wurtzite hexagonal phase). The planes correspond to d-spacing standards of 2.80, 2.59, 2.46, 1.90, 1.62, 1.47, 1.40, 1.37 and 1.35 Å, appropriately.

The crystallite sizes of Zr−AC, Ni−AC and Zn−AC were estimated by using the Scherer's equation [14]:

$$t = \frac{0.94\lambda}{\beta \cos\theta} \tag{2}$$

where $t$ is the crystallite size, $\lambda$ is the X-ray wavelength; $\theta$ is the Bragg diffraction angle; and $\beta$ is the peak width at full width half maximum. The estimated crystallite sizes of Zr−AC, Ni−AC and Zn−AC are in the range of 6−40 nm.

### 3.2 Morphology of Zr−AC, Ni−AC and Zn−AC

HR-SEM images of AC, Zr−AC, Ni−AC and Zn−AC are shown in Fig. 2. Figure 2(a) displays well-formed porous structure on the surface of AC. These pores are crucial in the adsorption and transportation of dye molecules. Figure 2(b) shows $ZrO_2$ nano-spheres present on the walls of the pores and on the surface of the carbon support. Figure 2(c) shows the presence of NiO spheres like nanostructures on the walls and within the pores of the activated carbon. Figure 2(d) shows the presence of ZnO nano-rods on the walls of the pores and on the surface of the carbon support.

### 3.3 XPS analysis

Figure 3(a) shows the constituent peaks of Zr−AC, Ni−AC and Zn−AC. Figure 3(b) reveals the profile of Zr 3d electron, a doublet of the Zr $3d_{5/2}$ and $3d_{3/2}$ peaks from the $Zr^{4+}$ states, which are at 183.8 and 186.2 eV, respectively, and they confirm the presence of $Zr^{4+}$ in Zr−AC [15]. Figure 3(c) shows the profile of Ni 2p electron, a doublet of the Ni $2p_{3/2}$ and $2p_{1/2}$ peaks from the $Ni^{2+}$ states, which are at 855.1 and 873.3 eV, respectively, as well as their corresponding shake-up resonances at 861.1 and 880 eV. These peaks are assigned to oxidized nickel in a dispersed phase, and they confirm the presence of $Ni^{2+}$ in Ni−AC [16]. Figure 3(d) shows the profile of Zn 2p electron, a doublet of the Zn $2p_{3/2}$ and Zn $2p_{1/2}$ peaks from the $Zn^{2+}$ states, which are at 1044 and 1022.5 eV, respectively, as well as their corresponding shake-up resonances at 1023 and 1047 eV [17].

Figures 4(a)−(c) show the O 1s core-level spectra of Zr−AC, Ni−AC and Zn−AC. Deconvolution of the O 1s peak in Zr−AC and Ni−AC, gives rise to two peaks of 530.9, 532.8 eV and 531, 532.9 eV, respectively. However, Zn−AC gives rise to three components centered at 527−534 eV, 531−540 eV and 535−539 eV. The peak at 531 eV implies the adsorbed oxygen on the vacancy sites of samples, it is associated with the $O^-$ sub-lattice and further it corresponds to the carbonyl oxygen atoms [18]. The peak at 532.9 eV affirms the

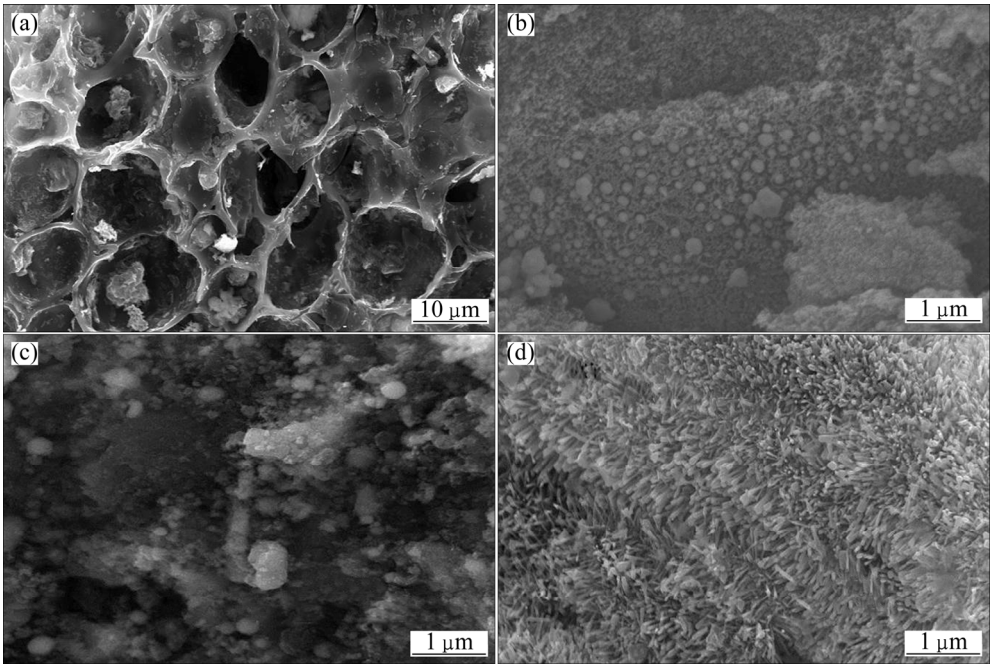


**Fig. 2** HR-SEM images of AC (a), Zr−AC (b), Ni−AC (c) and Zn−AC (d)

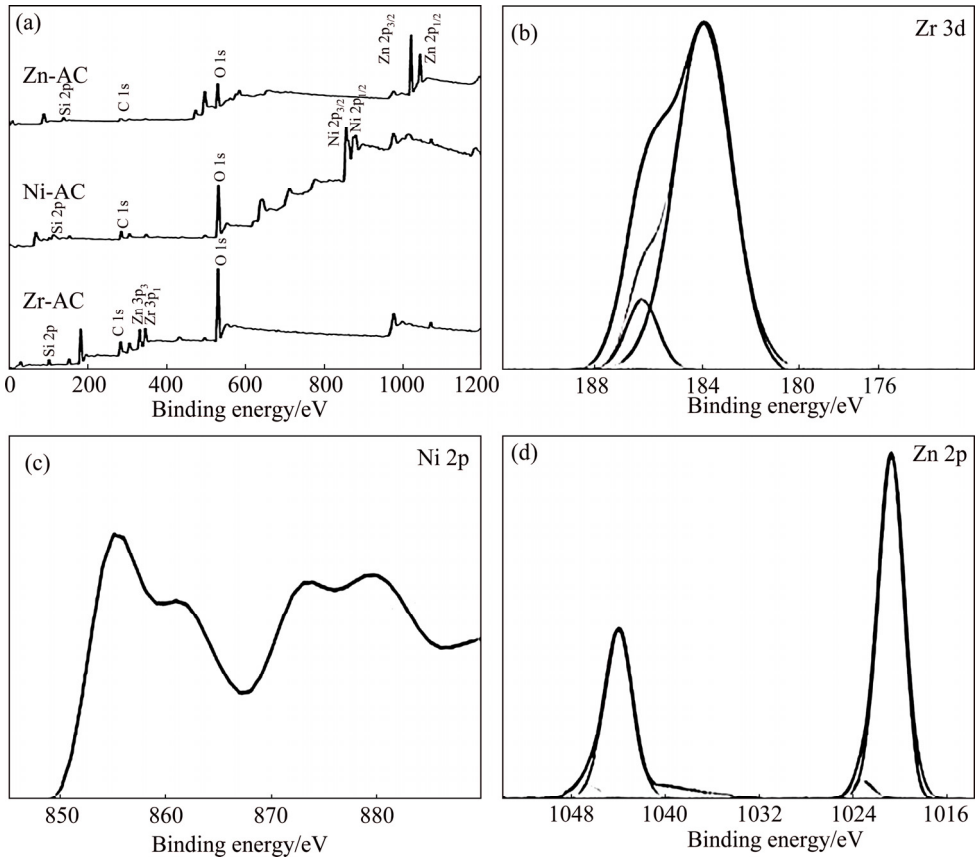


**Fig. 3** XPS profiles of wide spectra of Zr−AC, Ni−AC and Zn−AC (a), Zr 3d (b), Ni 2p (c) and Zn 2p (d)

presence of carbonyl oxygen atoms in esters, amides and anhydrides, as well as oxygen atoms in hydroxyls or ethers [19]. Additionally, it signifies the lattice oxygen-deficiency, and the surface bonded O—H or $O_2$ [20]. Besides, the binding energy of O 1s region showed an increase for Zr−AC, Ni−AC and Zn−AC as compared with pure $ZrO_2$, NiO and ZnO, as reported in Ref. [21]. The increase in the binding energy may be due to the capture of corresponding metal on carbon surface and the surface interaction between carbon and metal atoms [10].

The high-resolution XPS spectra of the C 1s region of Zr−AC, Ni−AC and Zn−AC are exhibited in Figs. 4(d)−(f), and the peak at 284.4 eV matches the $sp^2$ carbon bonding in graphitic carbon [22]. The peak at 286.2 eV is attributed to carbonyl and carboxylic groups [23]. The peak at 289 eV is attributed to the carbonyl, quinine groups, lactone or ester groups [24]. Moreover, an extra peak at high binding energy of about 293.9 eV is attributed to $\pi\rightarrow\pi^*$ transitions [25]. It can also be referred to C═C—O surface group [26].

### 3.4 Optical analysis

The diffuse reflectance spectra of Zr−AC, Ni−AC and Zn−AC in the range of 200−800 nm at room temperature were examined for their optical absorption properties. The reflectance spectra were analyzed using a modified Kubelka−Munk function $F(R)$ [27], estimated from the following equation:

$$F(R)=(1-R)^2/(2R) \quad (3)$$

where $R$ is the reflectance. A graph was plotted between $[F(R)h\upsilon]^2$ and $h\upsilon$, and the intercept value obtained corresponds to the band gap energy. The band gaps of Zr−AC, Ni−AC and Zn−AC evaluated using the modified Kubelka−Munk function are 4.81, 3.24 and 3.17 eV, respectively (Fig. 5).

The Zr−AC, Ni−AC, and Zn−AC samples show smaller band gap as compared with the pure $ZrO_2$ (5.00 eV), NiO (3.52 eV) and ZnO (3.30 eV). This red shift in Zr−AC, Ni−AC and Zn−AC samples band gap could be due to the quantum confinement experienced by the well dispersed $ZrO_2$, NiO and ZnO on the carbon matrix, thus leading to lower crystallite size, which is in accordance with XRD results [28]. This effect is likely due to the chemical defects or vacancies present in the intergranular regions generating new energy level to reduce the band gap energy [29]. The diffuse reflectance spectra vividly show that the Zr−AC, Ni−AC and Zn−AC samples are probable photocatalysts, which can perform efficiently under UV radiation.

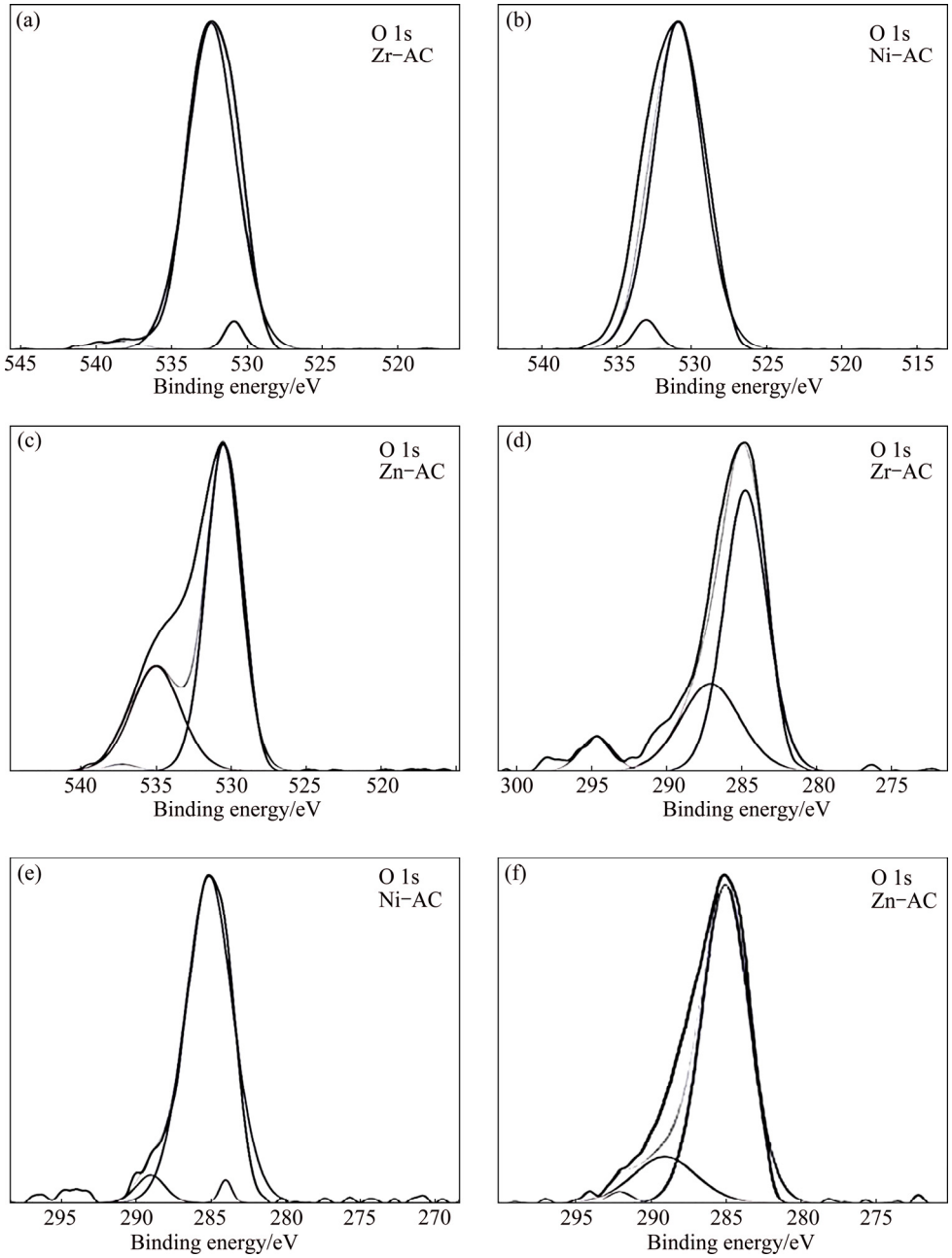


**Fig. 4** XPS patterns of O 1s (a−c) and C 1s (d−f) of Zr−AC, Ni−AC and Zn−AC, respectively

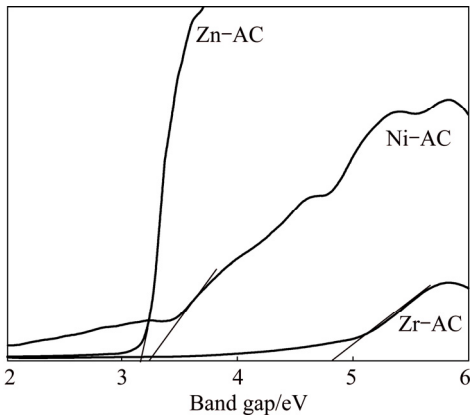


**Fig. 5** Diffuse reflectance spectra of Zr−AC, Ni−AC and Zn−AC

### 3.5 BET analysis

The porous structures of AC, Zr−AC, Ni−AC and Zn−AC were studied by using nitrogen adsorption at 77 K. The nitrogen isotherms of the AC, Zr−AC, Ni−AC and Zn−AC are plotted in Fig. 6.

The surface areas of the AC, Zr−AC, Ni−AC and Zn−AC are 446.44, 423.86, 404.24 and 247.76 $m^2/g$, respectively. The reduction in the surface areas of Zr−AC, Ni−AC and Zn−AC samples implies that the loading of corresponding metal oxides has taken place on the carbon matrix.

The AC, Zr−AC and Ni−AC samples show Type I and Type IV isotherms behaviour because they have a round knee at a relative pressure of $0.05<P/P_0<0.15$, and

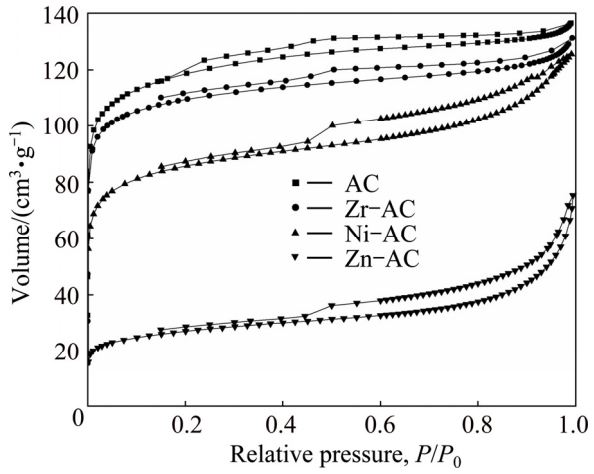


**Fig. 6** Nitrogen adsorption/desorption isotherms of AC, Zr−AC, Ni−AC and Zn−AC

exhibit hysteresis loop, corresponding to the mesopore structure. The isotherm of the Zn−AC exhibits Type IV curve, and this is the typical characteristic of mesoporous and macro-porous materials [30].

### 3.6 Photocatalytic activity

#### 3.6.1 Preliminary study of TDW photocatalytic degradation

The photocatalytic degradation of TDW (1150 mg/L COD) with AC, Zr−AC, Ni−AC and Zn−AC catalysts was carried out and their photocatalytic ability was estimated from rate of COD reduction (PCR) under 365 nm UV light irradiation. COD reduction affirms the elimination of the organic materials in the TDW and the color minimization [31]. The effect of Zr−AC, Ni−AC and Zn−AC composites on TDW was studied by UV−Vis spectroscopy (Fig. 7). The peak observed at 483 nm was caused by organic pollutants in wastewater, and it

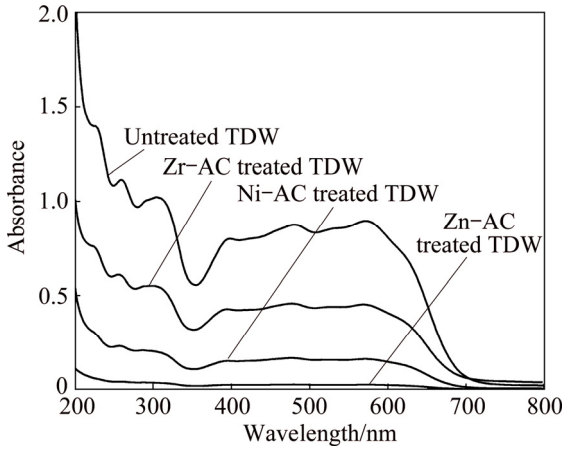


**Fig. 7** UV−Vis spectra of untreated TDW, Zr−AC treated TDW, Ni−AC treated TDW and Zn−AC treated TDW ($t$=180 min, pH=2, $\rho$(TDW)=1150 mg/L COD, catalyst dose=1.0 g, $\lambda$=365 nm)

decreased during photocatalytic degradation and a complete mineralization of TDW was obtained for Zn−AC.

#### 3.6.2 Photocatalytic activity of Zr−AC, Ni−AC and Zn−AC

In order to calculate the kinetics of TDW photocatalytic degradation, a general pseudo first order kinetics for TDW degradation was considered.

$$d\rho(TDW)/dt = -k_{app}\rho(TDW) \quad (4)$$

where $k_{app}$ is the apparent first order rate constant of TDW degradation, $\rho$(TDW) is the concentration of TDW at any instant time, $t$. The apparent rate constant ($k_{app}$) takes into account several in-between processes of adsorption, oxidation, and desorption. The concentration profile of TDW degradation can be represented as

$$\rho(TDW)=\rho(TDW)_0 \exp(-k_{app}t) \quad (5)$$

The data fitting was carried out for all the photocatalytic degradation studies to interpret the degradation in terms of the pseudo first order kinetics.

The effects of $ZrO_2$, NiO, ZnO, Zr−AC, Ni−AC and Zn−AC on the rate of TDW are shown in Fig. 8.

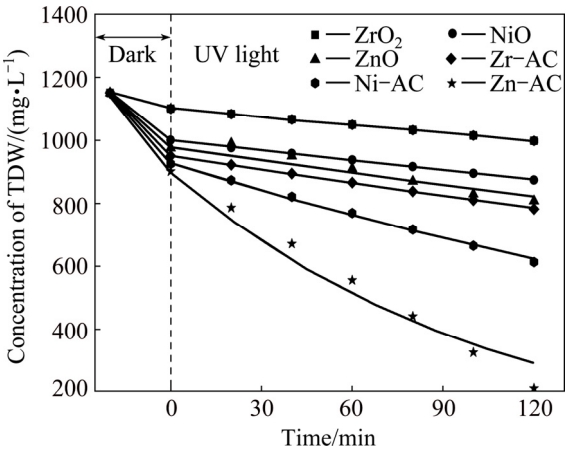


**Fig. 8** Effects of $ZrO_2$, NiO, ZnO, Zr−AC, Ni−AC and Zn−AC on rate of TDW degradation ($t$=120 min, pH=2, $\rho$(TDW)= 1150 mg/L COD, catalyst dose=1.0 g, $\lambda$=365 nm)

$ZrO_2$, NiO, ZnO, Zr−AC, Ni−AC and Zn−AC samples were able to degrade to 13%, 24%, 29%, 32%, 47% and 82%, correspondingly. The apparent first order rate constants of TDW degradation obtained for the above samples were $8.02\times10^{-4}$ min$^{-1}$, $0.11\times10^{-2}$ min$^{-1}$, $0.14\times10^{-2}$ min$^{-1}$, $0.31\times10^{-2}$ min$^{-1}$, $0.52\times10^{-2}$ min$^{-1}$ and $0.90\times10^{-2}$ min$^{-1}$, respectively. The rate constants of Zr−AC, Ni−AC and Zn−AC are higher than those of their corresponding metal oxides.

The effects AC, Zr−AC, Ni−AC and Zn−AC on the rate of TDW are shown in Fig. 9. The rate constant of Zn−AC is three times higher that of Zr−AC, this is because of the 365 nm UV radiation, which suits the

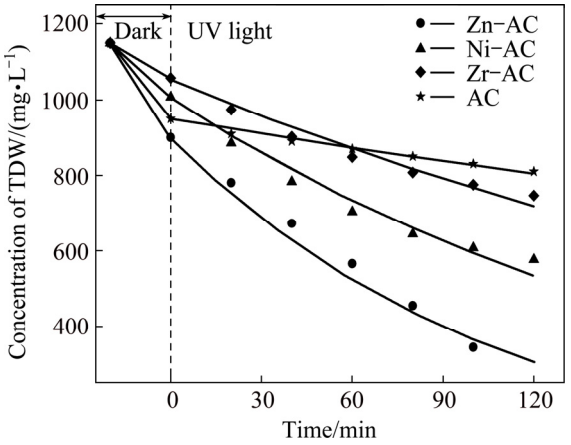


**Fig. 9** Effects of Zr−AC, Ni−AC and Zn−AC on rate of TDW degradation ($t$=120 min, pH=2, $\rho$(TDW)=1150 mg/L COD, catalyst dose=1.0 g, $\lambda$=365 nm)

band gap of Zn−AC and this applies for the photocatalytic efficiency of Ni−AC. Moreover, the ZnO nano-rods morphology is also responsible for higher photocatalytic efficiency of Zn−AC.

In rod-like morphology, the Zn-terminated (001) and O-terminated (001) polar faces are facile to adsorb oxygen molecules and $OH^-$ ions, which results in greater generation rate of $H_2O_2$ and OH• radicals, and thus enhancing the efficiency of Zn−AC. Further, it can be attributed to the presence of high concentration of oxygen vacancies, which lower the recombination between photogenerated electrons and holes, by serving as electron traps [32].

AC is a semiconductor, and it favours the photocatalytic activity. BOEHM [33] reported that when the photon from UV light falls on AC, it generates electron–hole pairs, due to the promotion of electrons from the valence to the conduction band. The electrons advance throughout the $sp^2$ hybridized layers and reach molecules of the absorbed species and oxygen molecules. The electrons in turn reduce the adsorbed $O_2$ to set superoxide radicals, which further, react with the water molecule and initiate the generation of oxidizing radical groups, which eventually degrade the organic matter. Besides, the presence of adsorbed oxygen on AC surface shuns the recombination of the electron with the positive hole, favoring the interaction between the water molecule and the positive hole, and thus expanding the capacity of the photocatalytic process.

The degradation ability in Zr−AC, Ni−AC and Zn−AC, is due to the synergy between the metal oxides and carbon support. The synergy mechanism is shown in Fig. 10.

When $ZrO_2$, NiO, ZnO nanoparticles are irradiated with photons, electron−hole pairs are generated. The photo-generated electrons reduce $O_2$ which are adsorbed on the catalyst surface and they are further dissolved in water to form superoxide radical ($^{\bullet}O_2^-$). The photo-generated holes directly oxidize the dye molecules and react with $OH^-/H_2O$ to create the eminently oxidizing hydroxyl radicals ($OH^{\bullet}$). AC as a support can behave as an effective electron propagation site, since it displays excessive electrical conductivity, and enormous electron storage capacity, with respect to the high specific surface area. AC as a support performs two important roles as a beneficiary and emissary of propagated electrons of $ZrO_2$, NiO, ZnO nanoparticles and definitely controls the charge recombination [34]. As well, due to the solid synergy between AC and $ZrO_2$, NiO, ZnO nanoparticles, the flow of transmitted electrons between the AC and the conduction band of $ZrO_2$, NiO, ZnO nanoparticles is raised. $ZrO_2$, NiO, ZnO nanoparticles are superior electron givers, and carbon materials are relatively good electron receivers, the synergistic effects between these components competently retard the charge recombination. The intermingling of the oxygen vacant sites, structural defects of $ZrO_2$, NiO and ZnO nanoparticles along with electron propagation capacity and the existence of surface oxygen on AC guide to long-term light absorption, held up charge recombination, and sustenance, which favor the advancement of the photocatalytic activity of Zr−AC, Ni−AC, and Zn−AC [35]. Zn−AC showed superior synergy effect and photocatalytic activity, which was considered for further investigation.

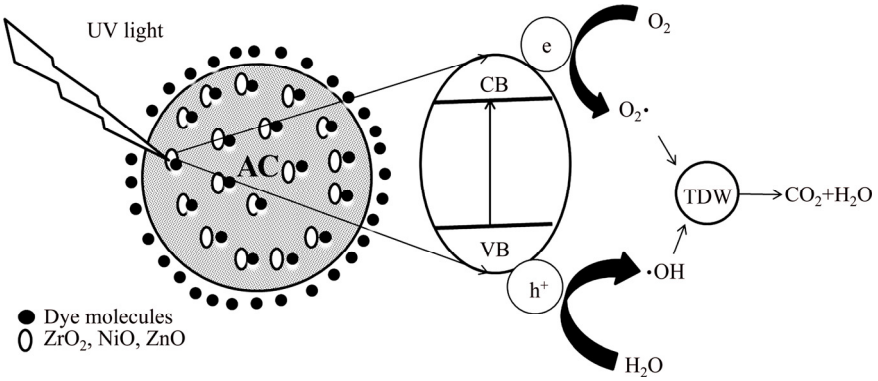


**Fig. 10** Synergy mechanism on surface of Zr−AC, Ni−AC and Zn−AC (CB—Conduction band; VB—Valence band)

3.6.3 Effect of Zn−AC dosage

The effect of Zn−AC dosage on the photocatalytic degradation rate of TDW is illustrated in Fig. 11.

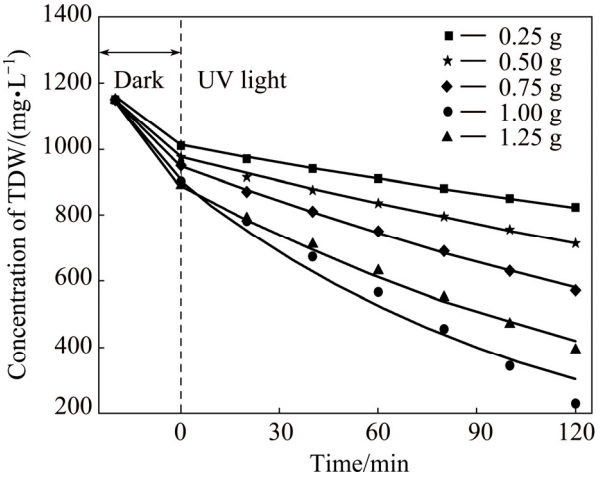


**Fig. 11** Effect of Zn−AC dosage on photocatalytic degradation of TDW ($t$=120 min, $\rho$(TDW)=1150 mg/L COD,$\lambda$=365 nm)

Higher Zn−AC dosage provides additional sites for generation of active radical, thereby enhancing the rate of reaction. The rate constants for Zn−AC dosages (0.25, 0.5, 0.75, 1.0 and 1.25 g) were $0.17\times10^{-2}$ min$^{-1}$, $0.28\times10^{-2}$ min$^{-1}$, $0.41\times10^{-2}$ min$^{-1}$ , $0.90\times10^{-2}$ min$^{-1}$ and $0.62\times10^{-2}$ min$^{-1}$, respectively. The increase in Zn−AC dosage from 0.25 to 1.0 g resulted in almost five times increase in the rate of degradation; however, a further increase of Zn−AC dosage to 1.25 g decreased the rate of degradation. Zn−AC dosage of 1.0 g was able to degrade to about 82% but 1.25 g of catalyst dosage was able to degrade only 71%. This shows that 1.0 g of Zn−AC is the optimum catalyst dosage for the photocatalytic degradation of TDW.

3.6.4 Effect of pH

The effect of pH on the photodegradation rate of TDW is exhibited in Fig. 12.

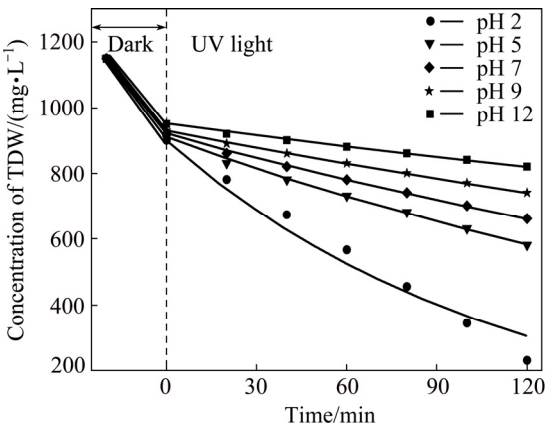


**Fig. 12** Effect of pH on photocatalytic degradation of TDW ($t$=120 min, dose=1.0 g, $\rho$(TDW)=1150 mg/L COD, $\lambda$=365 nm)

The effect of pH on the photodegradation of TDW was studied in the pH range of 2−12. The photodegradation of TDW decreased from pH 2 to 12. The rate constants for effect of pH (2, 5, 7, 9, 12) were $0.90\times10^{-2}$ min$^{-1}$, $0.37\times10^{-2}$ min$^{-1}$, $0.27\times10^{-2}$ min$^{-1}$, $0.19\times10^{-2}$ min$^{-1}$, and $0.12\times10^{-2}$ min$^{-1}$, respectively. The zero point charge ($pH_{ZPC}$) of Zn−AC is 8.40 and the surface is positively charged in acidic solution ($pH<pH_{ZPC}$) and negatively charged in alkaline solution ($pH>pH_{ZPC}$) [36]. TDW is a negatively charged dye and therefore the electrostatic attraction between the dye molecules and Zn−AC is greatly improved at pH 2. Likewise, when the medium shifts into basic, ion dipole combat between the negatively charged catalyst surface and the negatively charged dye molecules is likely at a higher pH [37]. This is true for TDW, which displayed diminished photocatalytic degradation at high alkalinity.

3.6.5 Reusability of Zn−AC

The reusability of the Zn−AC is an important factor for industrial applications, so the sample was analyzed for reusability. Photocatalytic experiments were carried out under the optimum reaction conditions using Zn−AC five times. After each reaction, Zn−AC was recovered from the reaction mixture by filtration and washed with distilled water several times to remove any TDW components adsorbed on the surface of the catalyst. The effect of run times on the TDW degradation over Zn−AC is shown in Fig. 13.

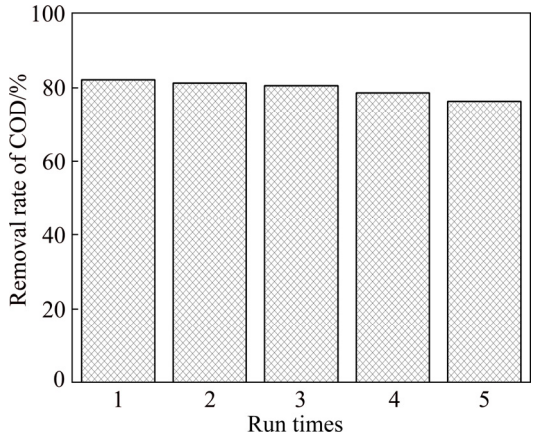


**Fig. 13** Effect of run times on TDW degradation over Zn−AC ($t$=120 min, pH=2, $\rho$(TDW)=1150 mg/L COD, catalyst dose=1.0 g, $\lambda$=365 nm)

The degradations of TDW for the five successive cycles of Zn−AC were 82.14%, 81.22%, 80.54%, 78.62%, and 76.32%, respectively. The marginal decrease in the photocatalytic efficiency after five cycles is attributed to the saturation of the carbon support with contaminants. The results ascertain that Zn−AC is a reusable photocatalyst for the degradation of TDW.

## 4 Conclusions

Exceptionally optically active Zn−AC photocatalyst was fabricated by microwave irradiation and characterized with XRD, SEM, XPS, BET, and UV−Vis DRS. The photocatalytic efficiency was investigated for the degradation of TDW and the efficiency of the examined catalyst follows the order of Zn−AC>Ni−AC> Zr−AC. The photocatalytic efficiency of ZnO is remarkably improved by the synergistic effects of AC and ZnO. The photodegradation of TDW follows the pseudo first order kinetics, and Zn−AC rate of degradation is three times that of Zr−AC. The optimized reaction conditions for the photocatalytic degradation are initial TDW concentration of 1150 mg/L COD, pH=2, $\lambda$=365 nm and catalyst dose=1.0 g. Under the optimum reaction conditions, 82% COD reduction was obtained within 120 min of irradiation. Zn−AC is a reusable photocatalyst and can be used five times without phenomenal drop in its efficiency.

## Acknowledgements

The authors duly acknowledge the encouragement and financial support rendered by the Salesians of Don Bosco, Dimapur Province, Nagaland, North East India.

## References

[1] DIVYA J, PARAGA D, VENUGOPAL B R, SRINIVASAN C, GIRIDHAR M. Transition metal oxide loaded MCM catalysts for photocatalytic degradation of dyes [J]. Journal of Chemical Sciences, 2012, 124: 385−393.

[2] ZENG Meng-xiong, LI You-ji, MA Ming-yuan, CHEN Wei, LI Lei-yong. Photocatalytic activity and kinetics for acid yellow degradation over surface composites of $TiO_2$-coated activated carbon under different photocatalytic conditions [J]. Transactions of Nonferrous Metals Society of China, 2013, 23(4): 1019−1027.

[3] ZHANG Li, YAN Jian-hui, ZHOU Min-jie, YU Yan-ping, LIU Ye, LIU You-nian. Photocatalytic degradation and inactivation of *Escherichia coli* by ZnO/$ZnAl_2O_4$ with hetero nanostructures [J]. Transactions of Nonferrous Metals Society of China, 2014, 24(3): 743−749.

[4] JIA Zhi-gang, PENG Kuan-kuan, LI Yan-hua, ZHU Rong-sun. Preparation and photocatalytic performance of porous ZnO microrods loaded with Ag [J]. Transactions of Nonferrous Metals Society of China, 2012, 22(4): 873−878.

[5] LUO Qiang, CAI Qi-zhou, LI Xin-wei, PAN Zhen-hua, LI Yu-jie, CHEN Xi-di, YAN Qing-song. Preparation and characterization of $ZrO_2$/$TiO_2$ composite photocatalytic film by micro-arc oxidation [J]. Transactions of Nonferrous Metals Society of China, 2013, 23(10): 2945−2950.

[6] ZENG Meng-xiong, LI You-ji, MA Ming-yuan, CHEN Wei, LI Lei-yong. Photocatalytic activity and kinetics for acid yellow degradation over surface composites of $TiO_2$-coated activated carbon under different photocatalytic conditions [J]. Transactions of Nonferrous Metals Society of China, 2013, 23(4): 1019−1027.

[7] DONG Shuang-shi, ZHANG Jian-bin, GAO Lin-lin, WANG Yan-long, ZHOU Dan-dan. Preparation of spherical activated carbon-supported and $Er^{3+}$:$YAlO_3$-doped $TiO_2$ photocatalyst for methyl orange degradation under visible light [J]. Transactions of Nonferrous Metals Society of China, 2012, 22(10): 2477−2483.

[8] SURESH P, JUDITH VIJAYA J, JOHN KENNEDY L, Photocatalytic degradation of textile-dyeing wastewater by using a microwave combustion-synthesized zirconium oxide supported activated carbon [J]. Materials Science in Semiconductor Processing, 2014, 27: 482−493.

[9] SURESH P, JUDITH VIJAYA J, JOHN KENNEDY L. Synergy effect in the photocatalytic degradation of textile dyeing waste water by using microwave combustion synthesized zinc oxide supported activated carbon [J]. Reaction Kinetic Mechanism and Catalysis, 2014, 114: 767−780.

[10] SURESH P, JUDITH VIJAYA J, , BALASUBRAMANIAM T, JOHN KENNEDY L. Synergy effect in the photocatalytic degradation of textile dyeing waste water by using microwave combustion synthesized nickel oxide supported activated carbon [J]. Desalination and Water Treatment, DOI: 10.1080/19443994.2014.989276.

[11] SURESH P, JUDITH VIJAYA J, JOHN KENNEDY L, THINESH KUMAR R. Two stage-two step activation process for the fabrication of micro-mesoporous carbons from rice husk [J]. Journal of Bioprocess Engineering and Biorefinery, 2013, 2: 230−239.

[12] KEFAYAT U, SHU Y, LEI Z, ZE D, SOURAV S, WON C. Microwave assisted synthesis of a noble metal-graphene hybrid photocatalyst for high efficient decomposition of organic dyes under visible light [J]. Materials Science and Engineering B, 2014, 180: 20−26.

[13] SMITH J V. X-ray powder data file [M]. Pennsylvania: American Society for Testing Materials, 1960.

[14] CULLITY B D. Elements of X-ray diffraction [M]. Massachusetts: Addison-Wesley Publication Company, 1978.

[15] ZHANG N L, SONG Z T, WAN Q, SHEN Q W, LIN C L. Interfacial and microstructural properties of zirconium oxide thin films prepared directly on silicon [J]. Applied Surface Science, 2002, 202: 126−130.

[16] ANDREW P, BIESINGER M C, SMART R S C, MCINTYRE N S. Interpretations of XPS spectra of nickel metal and oxides [J]. Surface Science, 2006, 600: 1771−1779.

[17] WU M L, REN C Z. Active control of the anisotropic wettability of the carbon fiber reinforced carbon and silicon carbide dual matrix composites (C/C−SiC) [J]. Applied Surface Science, 2015, 327: 424−431.

[18] MACHOCKI A, IOANNIDES T, STASINSKA B, GAC W, AVGOUROPOULOS G, DELIMARIS D, GRZEGORCZYK W, PASIECZNA S. Manganese−lanthanum oxides modified with silver for the catalytic combustion of methane [J]. Journal of Catalysis, 2004, 227: 282−296.

[19] YU C C, CHEN Y L, HUNG C L. Surface chemistry of polyacrylonitrile and rayon-based activated carbon fibers after post-heat treatment [J]. Materials Chemistry and Physics, 2007, 101: 199−210.

[20] XUEFENG W, RONGKUN Z, ZONGWEN L, HOPUI H, JIANBIN X, SIMON P R. Structural, optical and magnetic properties of Co-doped ZnO nanorods with hidden secondary phases [J]. Nanotechnology, 2008, 19: 455702.

[21] GUANGMEI B, HONGXING D, JIGUANG D, YUXI L, WENGE Q, ZHENXUAN Z, XINWEI L, HUANGGEN Y. The microemulsion preparation and high catalytic performance of mesoporous NiO nanorods and nanocubes for toluene combustion [J]. Chemical Engineering Journal, 2013, 219: 200−208.

[22] AI L, ZHANG C, CHEN Z. Removal of methylene blue from aqueous solution by a solvothermal-synthesized graphene/magnetite composite [J]. Journal of Hazardous Materials, 2011, 192: 1515−1524.

[23] ALEXANDRE F, IRENE S M, XIAOXING K, GUSTAAF V T, JACQUES G, JEAN J P, WOLGANG D, CARLA B, CHRISTOPHER P. The interface between titanium and carbon nanotubes [J]. A European Journal of Chemical Physics and Physical Chemistry, 2009, 10: 1799−1804.
[24] CASTILLA C M, RAMON M V L, MARIN F C. Changes in surface chemistry of activated carbons by wet oxidation [J]. Carbon, 2000, 38: 1995−2001.
[25] OKPALUGO T I T, PAPAKONSTANTINOU P, MURPHY H, MCLAUGHLIN J, BROWN N M D. High-resolution XPS characterization of chemical functionalized MWCNTs and SWCNTs [J]. Carbon, 2005, 43: 153−161.
[26] BALAZS D J, TRIANDAFILLU K, CHEVOLOT Y, ARONSSON B O, HARMS H, DESCOUTS P, MATHIEU H. Surface modification of PVC endotracheal tubes by oxygen glow [J]. Surface and Interface Analysis, 2003, 35: 301−309.
[27] HAYS J, REDDY K M, GRACES N Y, ENGELHARD M H, SHUTTHANADAN V, LUO M, XU C, GILES N C, WANG C, THEVUTHASAN S, PUNNOOSE A. Effect of Co doping on the structural, optical and magnetic properties of ZnO nanoparticles [J]. Journal of Physics: Condensed Matter, 2007, 19: 266203.
[28] SATHISH M, VISWANATHAN B, VISWANATH R P. Alternate synthetic strategy for the preparation of CdS nanoparticles and its exploitation for water splitting [J]. International Journal of Hydrogen Energy, 2006, 31: 891−898.
[29] SONG X, GAO L. Facile synthesis of polycrystalline NiO nanorods assisted by microwave heating [J]. Journal of the American Ceramic Society, 2008, 91: 3465−3468.
[30] LI Guang-ci, GUAN Li-li, LIU Yun-qi, LIU Chen-guang. Template-free solvothermal synthesis of 3D hierarchical nanostructured boehmite assembled by nanosheets [J]. Journal of Physics and Chemistry of Solids, 2012, 73(9): 1055−1060.
[31] MUTHIRULAN P, MEENAKSHISUNDARAM M, KANNAN N. Beneficial role of ZnO photocatalyst supported with porous activated carbon for the mineralization of alizarin cyanin green dye in aqueous solution [J]. Journal of Advanced Research, 2013, 4: 479−484.
[32] SELVAM N C S, JUDITH VIJAYA J, JOHN KENNEDY L. Effects of morphology and Zr doping on structural, optical, and photocatalytic properties of ZnO nanostructures, [J] Industrial and Engineering Chemistry Research, 2012, 51: 16333−16345.
[33] BOEHM H P. Free radicals and graphite [J]. Carbon, 2012, 50: 3154−3157.
[34] WILSON N, ALMEIDA G, JOANA M. TEIXEIRA S, LUCIA R. RASSI D A. Decolorization and mineralization of reactive dyes by a photocatalytic process using ZnO and UV radiation [J]. Water Science and Technology, 2012, 66: 158−164.
[35] LUKA J C, KLEMENTOVA M, BEZDICK P, BAKARDIJEV S, SUBRT J, SZATMARY L, BASTLL Z, JIRKOVSKY. Influence of Zr as $TiO_2$ doping ion on photocatalytic degradation of 4-chlorophenol [J]. Applied Catalysis B: Environmental, 2007, 74: 83−91.
[36] ANANDAN S, VINU A, VENKATACHALAM N, ARABINDOO B, MURUGESAN V. Photocatalytic activity of ZnO impregnated Hβ and mechanical mix of ZnO/Hβ in the degradation of monocrotophos in aqueous solution [J]. Journal of Molecular Catalysis A: Chemical, 2006, 256: 312−320.
[37] TANG W Z, HUANG C P. Photocatalyzed oxidation pathways of 2, 4-dichlorophenol by CdS in basic and acidic aqueous solutions [J]. Water Research, 1995, 29: 745−756.

# 微波合成 Zr−AC, Ni−AC 和 Zn−AC 光催化降解印染废水

P. SURESH[1], J. JUDITH VIJAYA[1], L. JOHN KENNEDY[2]

1. Catalysis and Nanomaterials Research Laboratory, Department of Chemistry, Loyola College, Chennai 600034, India;
2. Materials Division, School of Advanced Sciences, VIT University, Chennai Campus, Chennai 600048, India

**摘 要**：采用微波照射法成功制备新型氧化锆、氧化镍和氧化锌负载活性炭纳米颗粒。采用 XRD、HR-SEM 和 BET 对合成纳米颗粒进行表征。利用 UV-Vis 漫反射光谱法研究 Zr−AC、Ni−AC 和 Zn−AC 复合材料的光学性能。验证了紫外光照射下印染废水的光催化效率。每隔一定时间观察印染废水的化学需氧量，以计算化学需氧量的去除率。结果表明，Zn−AC 复合材料具有明显的光催化性，这归因于紫外光区域吸光度的增大、染料分子的有效吸附能力、辅助电荷转移和电子−空穴对抑制重组。利用 Zn−AC 复合材料降解印染废水可以得到最大的降解率(82%化学需氧量去除率)。在 Zn−AC 复合材料表面设计一个可能实现的协同机制。Zn−AC 复合材料重复使用 5 次后，其催化活性无明显降低。

**关键词**：纳米结构；半导体；印染废水；光学性能；催化降解

**(Edited by Xiang-qun LI)**